ZOOLOGICAL RESEARCH

Assessment of mitochondrial function in metabolic dysfunction-associated fatty liver disease using obese mouse models

Qiong-Ya Zhao[1,2,#], Ling-Hong Ge[3,#], Kun Zhang[2,#], Hai-Feng Chen[2], Xin-Xin Zhan[2], Yue Yang[2], Qing-Lin Dang[2], Yi Zheng[2], Huai-Bin Zhou[2], Jian-Xin Lyu[2,*], He-Zhi Fang[2,*]

[1] *School of Laboratory Medicine*, *Hangzhou Medical College*, *Hangzhou*, *Zhejiang* 310053, *China*

[2] *Key Laboratory of Laboratory Medicine*, *Ministry of Education*, *Zhejiang Provincial Key Laboratory of Medical Genetics*, *College of Laboratory Medicine and Life Sciences*, *Wenzhou Medical University*, *Wenzhou*, *Zhejiang* 325035, *China*

[3] *Second Affiliated Hospital of Zhejiang Chinese Medical University*, *Hangzhou*, *Zhejiang* 310005, *China*

ABSTRACT

Metabolic dysfunction-associated fatty liver disease (MAFLD) is characterized by deregulated hepatic lipid metabolism; however, the association between MAFLD development and mitochondrial dysfunction has yet to be confirmed. Herein, we employed high-resolution respirometry, blue native polyacrylamide gel electrophoresis-based in-gel activity measurement and immunoblot analysis to assess mitochondrial function in obesity-induced mouse models with varying degrees of MAFLD. Results showed a slight but significant decrease in hepatic mitochondrial respiration in some MAFLD mice compared to mice fed a standard diet. However, the activities and levels of mitochondrial oxidative phosphorylation complexes remained unchanged during obesity-induced MAFLD progression. These results suggest that mitochondrial function, particularly oxidative phosphorylation, was mildly affected during obesity-induced MAFLD development. Moreover, transcriptome profiling of mouse and human liver tissues with varying degrees of MAFLD revealed that the decreased activation of mitochondria-related pathways was only associated with MAFLD of a high histological grade, whereas the major regulators of mitochondrial biogenesis were not altered in mice or humans during MAFLD development. Collectively, our results suggest that impaired hepatic mitochondrial function is not closely associated with obesity-induced MAFLD. Therefore, therapeutic strategies targeting mitochondria for the treatment of MAFLD should be reconsidered.

Keywords: Obesity; Mitochondria; Metabolic dysfunction-associated fatty liver disease; Hepatic steatosis; Steatohepatitis

INTRODUCTION

Metabolic dysfunction-associated fatty liver disease (MAFLD), originally termed nonalcoholic fatty liver disease, is

Received: 11 March 2020; Accepted: 21 July 2020; Online: 11 August 2020

Foundation items: This research was supported by the National Natural Science Foundation of China (Key Program: 81830071), Zhejiang Provincial Natural Science Foundation of China (LY19H040004 and Key Program: LR20H200001), and Zhejiang Provincial Health Science and Technology Plan (2015KYB238)

[#]Authors contributed equally to this work

*Corresponding authors, E-mail: jxlu313@163.com; FangH@wmu.edu.cn

DOI: 10.24272/j.issn.2095-8137.2020.051

characterized by excessive fat accumulation in the liver not associated with alcoholism (Eslam et al, 2020). In China, 29% of the population is affected by MAFLD (Zhou et al, 2019). Although it is generally believed that obesity is correlated with the development of MAFLD, lean individuals, particularly within Asian populations, are also affected (Younossi et al, 2018). The clinicopathological spectrum of MAFLD extends from simple steatosis or nonalcoholic fatty liver (NAFL) to nonalcoholic steatohepatitis (NASH), which can then progress to fibrosis, cirrhosis, and hepatocellular carcinoma (Kopec & Burns, 2011).

Previously, insulin resistance was considered the first hit for MAFLD development, causing excess lipolysis, followed by the release of a large amounts of free fatty acids (FFAs) into the liver and the development of simple steatosis (Fabbrini et al, 2008). The first hit makes the liver vulnerable to second hit stress factors, such as oxidative stress, lipid peroxidation, and proinflammatory cytokines, which can lead to more severe symptoms (Hijona et al, 2010). Recently, this multiple-hit hypothesis has been further developed to provide an improved interpretation of the pathological condition of MAFLD, suggesting that synergistic effects of multiple factors, including insulin resistance, adipose dysregulation, inflammation, and oxidative stress, are involved in the development of MAFLD (Tilg & Moschen, 2010). Although fat accumulation in the liver resulting from obesity and insulin resistance continues to be defined as the first hit, the contributions of and pathological mechanisms mediated by other factors in the progression of MAFLD remain incompletely understood.

One such factor includes decreased hepatic mitochondrial function, which is observed in obese patients with NASH (Garcia-Ruiz et al, 2013; Koliaki et al, 2015). Excessive FFAs can cause insulin resistance, which then generates elevated levels of acetyl coenzyme A through the mitochondrial β-oxidation pathway, which, in turn, leads to increased generation of NADH and $FADH_2$ via tricarboxylic acid (TCA) cycle flux. These both then serve as electron donors during oxidative phosphorylation (OXPHOS), resulting in enhanced generation of reactive oxygen species (ROS). The mitochondria then become damaged by ROS, causing a disruption in lipid homeostasis. Together, these processes trigger a perpetual cycle involving the production of FFAs and severe mitochondrial dysfunction, activating an inflammatory response and aggravating the progression of MAFLD (Bechmann et al, 2012b; Neuschwander-Tetri, 2010; Simoes et al, 2018). Specifically, reduced hepatic mitochondrial function has been observed in a sedentary, hyperphagic, obese Otsuka Long-Evans Tokushima fatty rat model (Rector et al, 2010); however, it was shown to exist prior to insulin resistance and hepatic steatosis, suggesting that mitochondrial dysfunction precedes the development of MAFLD (Bechmann et al, 2012a). High-fat diet (HFD)-induced liver steatosis does not affect the mitochondrial respiratory chain in mice (Franko et al, 2014). Furthermore, insulin sensitivity is reportedly increased in obese patients with and without type 2 diabetes following surgical intervention; however, the mitochondrial respiratory capacity is not affected, indicating weak correlation between insulin sensitivity and mitochondrial function (Lund et al, 2018). These studies suggest an uncertain association of mitochondrial dysfunction with progression of MAFLD.

In this study, we investigated the association between mitochondrial dysfunction and MAFLD progression via multi-time-point analysis of functional changes in mitochondria using a multi-dietary mouse model. *In vivo* results and transcriptomic analysis indicated that OXPHOS function decreased slightly during the development of MAFLD. Moreover, re-analysis of a public transcriptome dataset from human patients with various degrees of MAFLD provided further support for a mild association between mitochondrial dysfunction and MAFLD progression.

MATERIALS AND METHODS

Animals

All animal care and experimental protocols were approved by the Ethical Committee at Wenzhou Medical University. All animals were used in accordance with the procedures approved by the Animal Care and Use Committee of Wenzhou Medical University and complied with the Animals in Research: Reporting *In Vivo* Experiments (ARRIVE) guidelines.

SPF male B6 and D2 mice were purchased from Shanghai Slack Laboratory Animals Co., Ltd. (China) by the Animal Experimental Center of Wenzhou Medical University, where they were housed under specific pathogen-free conditions and a 12 h light/dark cycle. Five-week-old mice (n=6 per group) were randomly assigned to one of three groups and were fed one of the following diets: standard diet (SD) (Animal Experimental Center of Wenzhou Medical University), 60% HFD, and high-fat, high-fructose, high-cholesterol diet (HFFCD) (45% HFD supplemented with 1% cholesterol (Beijing Translation Technology, China) and high-fructose corn syrup equivalents (42 g/L glucose and fructose; 55% and 45%, respectively) in drinking water). Body weights were measured weekly at the same time of day during the feeding period. After 4, 8, 12, and 18 weeks on the different diets, the mice were euthanized.

During the last week of feeding, glucose and insulin tolerance tests were performed. Glucose tolerance tests were performed after 12 h of fasting using an intraperitoneal injection of glucose (1.5 g/kg). Glucose levels were then measured using a glucometer in blood collected via tail-vein sampling at 0, 15, 30, 60, 90, and 120 min post-injection. Insulin tolerance tests were performed after 6 h of fasting using an intraperitoneal injection of regular human insulin (0.75 IU/kg). Glucose levels were then measured using a glucometer in blood collected via tail-vein sampling at 0, 15, 30, 45, and 60 min post-injection.

Enzyme-linked immunosorbent assays (ELISAs)

Retro-orbital blood of mice was collected, and serum was separated via centrifugation at 2 000 *g* for 10 min at 4 °C to

measure the relative concentrations of alanine aminotransferase (ALT) and aspartate transaminase (AST) using ELISA kits (C009-2/C010-2; Nanjing Jiancheng, China) according to the manufacturer's instructions. Freshly harvested livers were washed with ice-cold phosphate-buffered saline (PBS) and then homogenized in PBS (9 mL/g tissue) using a glass homogenizer on ice. The homogenates were centrifuged for 5 min at 5 000 *g* at 4 °C to retrieve supernatants for measuring relative concentrations of triglycerides (TGs) (A110-1; Nanjing Jiancheng, China), nonesterified fatty acids (NEFAs) (A042-2; Nanjing Jiancheng, China), and 8-hydroxy-2′-deoxyguanosine (8-OHdG) (K4160-100; BioVision, USA) in liver tissue lysates using respective ELISA kits according to the manufacturer's instructions.

Histological and immunohistochemical analyses

Freshly harvested livers were washed with PBS, preserved in 4% paraformaldehyde, and then dehydrated. Tissue samples were embedded in paraffin, cut to a thickness of 5 μm, and stained with hematoxylin and eosin (H&E) solutions (C0105-1 and C0105-2, respectively; Beyotime, China). For Oil Red O (A600395-0050; Sangon Biotech, China) staining, liver samples were cleaned and embedded in paraffin, prior to dehydration with 30% sucrose for 48 h (V900116; Sigma-Aldrich, USA). Samples were then sectioned (10 μm thickness) using Cryostat Microm HM 525 (Thermo Fisher Scientific, USA). NASH severity (steatosis, hepatocyte ballooning, lobular inflammation, and portal inflammation) was measured as an MAFLD activity score in H&E-stained cross sections according to the standardized histological scoring system described previously (Kleiner et al, 2005). For each section, 10 randomly selected fields of view were analyzed by two pathologists. For immunohistochemical analysis of macrophage infiltration, liver sections were incubated with a primary anti-galectin-3 antibody (14979-1-AP; Proteintech Group, USA), followed by incubation with the corresponding secondary antibody. All sections were assessed using light microscopy (Nikon, Japan).

Measurement of oxygen consumption

Mitochondrial oxygen consumption was measured using a Clark-type electrode (Oroboros Instruments GmbH, Austria), as described previously (Silva & Oliveira, 2012). Firstly, mitochondria was extracted as follows. Liver tissues were homogenized with a glass homogenizer in buffer A (0.32 mol/L mannitol, 1 mmol/L EDTA, 10mmol/L Tris-HCl pH 7.4). The lysate was centrifuged for 5 min at 1 000 *g* at 4 °C. Discard the supernatant, and the pellet was suspended in the buffer A, the mitochondria was obtained after two times of centrifugation (2 min at 1 5000 *g* at 4 °C). Then 80 μg mitochondria was incubated in a test solution containing 2 mmol/L KH_2PO_4 and 2.5 mmol/L adenosine diphosphate (ADP) and then placed into a respirometry chamber. Two separate protocols were applied at 37 °C, and the oxygen flux rates were adjusted for mitochondrial concentrations. For the first protocol, 25 μL of a 5:1 mixture of 1 mol/L glutamate and 1 mol/L malate (complex I substrates), 2 μL of 1 mmol/L rotenone (complex I inhibitor), 10 μL of 1 mol/L succinate (complex II substrate), and 50 μL of 75 mg/mL 3-nitropropionic acid (complex II inhibitor) were sequentially added for the detection of complex-dependent oxygen respiration. The second protocol involved the consecutive addition of a mixture of complex I/II substrates, including 25 μL of 1 mol/L glutamate and 1 mol/L malate (5:1), 10 μL of 1 mol/L succinate (state 3), 2 μL of 100 mmol/L oligomycin (state o), and 2 μL of 1 mmol/L FCCP (state u).

Blue native polyacrylamide gel electrophoresis (PAGE), sodium dodecyl sulfate (SDS)-PAGE, and immunoblotting

Total proteins were extracted from liver tissues using radioimmunoprecipitation assay lysis buffer (Cell Signaling Technology, USA). Mitochondrial membrane proteins were extracted from hepatic mitochondria using 2% digitonin (Merck KGaA, Germany) for the isolation of OXPHOS super-complexes. Next, 100 μg of protein was mixed with 0.5% Blue G-250 (Sigma, USA) and 5% glycerol and separated using 3%–11% gradient blue native gel electrophoresis, as described previously (Sun et al, 2016). For the complex I in-gel activity assay, gels were soaked in an assay buffer containing 25 mg of nitroblue tetrazolium (NBT; Sigma, USA) and 10 μL of 1 mg/mL reduced NADH (Sigma, USA) in 10 mL of 5 mmol/L Tris-HCl (pH 7.4) for approximately 0.5 h. For complex II in-gel activity assay, gels were soaked in an assay buffer containing 1 mol/L sodium succinate (Sigma, USA), 8 μL of 250 mmol/L dimethyl sulfoxide (Sigma, USA), and 25 mg of NBT in 10 mL of 5 mmol/L Tris-HCl (pH 7.4) for approximately 0.5 h. For complex IV assay, gels were soaked in an assay buffer containing 50 mmol/L NaH_2PO_4 (pH 7.4), 5 mg of 3,3'-diaminobenzidine tetrahydrochloride hydrate (Sigma, USA), and 10 mg of cytochrome c (Sigma, USA) for 2 h. For complex V assay, gels were soaked in an assay buffer containing 10 mL of 35 mmol/L Tris-HCl (pH 8.3), 270 mmol/L glycine, 14 mmol/L $MgSO_4$ (Sigma, USA), 20 mg of $Pb(NO_3)_2$, and 4.4 mg of ATP (Sigma, USA) for 2 h. Proteins were separated using blue native PAGE or SDS-PAGE and then transferred onto 0.45 μm polyvinylidene difluoride membranes (Bio-Rad, USA). The membranes were probed with anti-Grim19 (1:1 000, ab110240; Abcam, USA), anti-SDHA (1:1 000, ab14715; Abcam, USA), anti-UQCRC2 (1:1 000, ab14745; Abcam, USA), anti-MT-COI (1:1 000, ab14705; Abcam, USA), anti-ATP5A (1:1 000, ab14748; Abcam, USA), anti-SOD1 (1:1 000, ab16831; Abcam, USA), anti-SOD2 (1:1 000, sc18503; Santa Cruz Biotechnology, USA), anti-PRDX1 (1:1 000; ab184247, Abcam, USA), anti-Trx (1:1 000, #2429; Cell Signaling Technology, USA), anti-CAT (1:1 000, #14097; Cell Signaling Technology, USA), anti-glyceraldehyde 3-phosphate dehydrogenase (GAPDH) (1:2 000, sc32233; Santa Cruz Biotechnology, USA), and anti-DNP (1:1 000, #14681; Cell Signaling Technology, USA) antibodies, followed by incubation with a horseradish peroxidase-conjugated anti-rabbit or anti-mouse IgG secondary antibody (1:2 000; Cell Signaling Technology, USA). Signals were detected using the Super Signal West Pico chemiluminescent substrate (Thermo Fisher Scientific,

USA). Integrated optical density quantification was performed using Gel-Pro Analyzer v4.0 (Media Cybernetics, USA).

Mouse transcriptome profiling

Total RNA was isolated from liver tissues of the HFD-, HFFCD-, and SD-fed mice (n=5 per group) using an RNeasy mini extraction kit (Qiagen, USA), and mRNA was purified from 20 μg of total RNA using poly-T-attached magnetic beads. Library construction and sequencing were performed using an Illumina HiSeq 2000 platform (Illumina, USA) by the Novogene Corporation (China), as described previously (Fang et al, 2018). To obtain clean reads, low-quality reads and reads containing adaptors or adaptor sequences and poly-N were removed from the raw data. Reference genome and gene model annotation files were downloaded directly from genome websites. The reference genome was built, and paired-end clean reads were aligned to the reference genome using STAR v2.5.1b. FeatureCounts was used to count the reads mapped to each gene. The DESeq2 R package was used to normalize gene counts and identify differentially expressed genes (DEGs) between HFD- and HFFCD-fed mice with SD-fed mice. Prior to DEG analysis, which was conducted using the ggord package in R, principal component analysis (PCA) was performed using data for each comparison group (HFD-/HFFCD-fed mice relative to paired SD-fed mice), generated for different time points to ensure that the data were usable. Genes showing an adjusted P-value of ≤0.05 were considered DEGs. The clusterProfiler package in R was used to perform Gene Ontology (GO) and Kyoto Encyclopedia of Genes and Genomes (KEGG) pathway enrichment analyses for up-regulated or down-regulated genes. Pathway heatmaps were generated using the pheatmap package. For model analysis, we included genes differentially expressed in samples from at least three consecutive time points. The fold-change of each gene in each group was used as the input data. Raw data were submitted to the NGDC Genome Sequence Archive (GSA) under accession No. CRA002935.

Transcriptome profiling of human data

RNA sequencing raw count data of human liver tissues from individuals of a healthy weight (normal controls (NCs), n=14), obese weight (n=12), and with simple steatosis (NAFL) (n=15) or NASH (n=16) were obtained from the Gene Expression Omnibus (GEO) database (GSE126848). The EdgeR package was used to normalize gene counts and identify DEGs. Genes showing an adjusted P-value of ≤0.05 were considered DEGs. The ggfortify package was used for PCA. Pathway analysis was performed as described for mouse data.

Statistical analysis

All experiments were performed a minimum of three times for each group. Data are presented as mean±standard error of the mean (*SEM*). Significance was estimated using an independent Student's t-test with IBM SPSS Statistics 22 (https://www.ibm.com/support/pages/spss-statistics-220-available-download). Figures were created using GraphPad Prism 7 (https://www.graphpad.com/). Significance was set at P<0.05.

RESULTS

Establishment of diet-induced mouse models of NASH

Five-week-old male mice from two phylogenetically distant strains, i.e., C57BL/6J (B6) and DBA/2J (D2), were fed a HFD, HFFCD, or SD diet for 4, 8, 12, and 18 weeks, followed by phenotypic and molecular characterization (Figure 1A). As shown in Figure 1B, mice on the HFD and HFFCD diets showed significantly higher body weights than the SD-fed controls, with the B6/HFD-fed mice gaining the most weight. From week 4, the D2/HFD- and B6/HFFCD-fed mice exhibited significantly higher hepatic levels of TGs than the SD-fed mice, with persistent trends through to the end of the study. The B6/HFD-fed mice also showed significantly higher TG levels than the B6/SD-fed mice until 18 weeks (Figure 1C). The D2/HFD-fed mice had higher hepatic levels of NEFAs compared to the D2/SD-fed mice at 4 and 8 weeks, whereas the B6/HFFCD-fed mice showed significantly higher hepatic NEFA levels compared to the B6/SD-fed mice at 4, 8, and 18 weeks. No differences were observed in the hepatic NEFA levels between the B6/HFD- and B6/SD-fed mice throughout the study (Supplementary Figure S1A). Serum ALT levels remained unchanged in the HFD- and SD-fed mice during the feeding period but were significantly higher in the B6/HFFCD-fed mice compared to the B6/SD-fed mice at 18 weeks (Supplementary Figure S1B). No significant differences were observed in the serum AST levels between the HFD- or HFFCD- and SD-fed mice at any time point (Supplementary Figure S1C), indicating that consuming a HFD or HFFCD diet for 18 weeks did not affect serum AST levels in either B6 or D2 mice. In addition, glucose tolerance tests showed significantly higher glucose levels in mice fed HFD or HFFCD compared to those fed SD from 4 weeks onward (Figure 1D, Supplementary Figure S1D–F). These findings indicate that HFD induced insulin resistance throughout the experimental period. Moreover, the D2/HFD-fed mice showed lower insulin sensitivity compared to the SD-fed mice at 8 and 12 weeks (Figure 1E, Supplementary Figure S1G) Although no significant differences were observed until 18 weeks between the B6/HFD- and SD-fed mice (Figure 1E, Supplementary Figure S1H), insulin sensitivity was significantly lower in the B6/HFFCD-fed mice compared to the SD-fed mice at 4 and 18 weeks (Figure 1F, Supplementary Figure S1I).

We subsequently evaluated the pathological changes in liver tissues of mice on different diets. A slight accumulation of lipid droplets was observed in the Oil Red O-stained liver tissues of HFD- or HFFCD-fed mice from 4 weeks, with a gradual increase to the end of the study (Supplementary Figure S1J). Immunostaining revealed increased macrophage infiltration in the HFD- and HFFCD-fed mice during the feeding period (Supplementary Figure S1K). Furthermore, H&E staining revealed hepatic steatosis and ballooning, accompanied by occasional inflammatory cell infiltration in

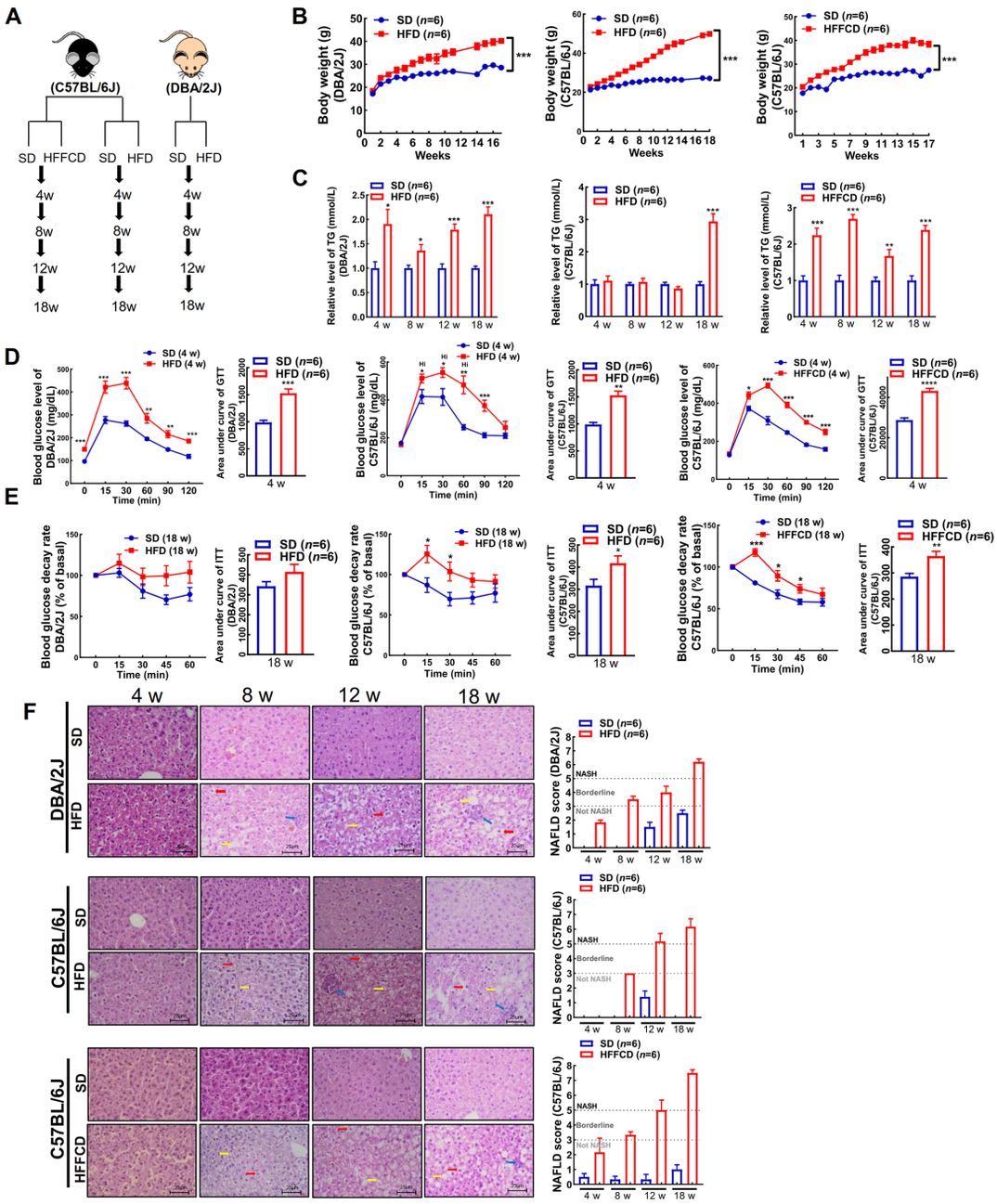

Figure 1 Establishment of diet-induced models of NASH

A: Schematic of study design. Mice from two phylogenetically distant strains (B6 and D2) were randomly divided into groups (n=6 per group) and fed different diets: i.e., high-fat diet (HFD), high-fat, high-fructose, high-cholesterol diet (HFFCD), and standard diet (SD). After 4, 8, 12, and 18 weeks of feeding, mice were euthanized for subsequent experiments. B: Body weights of mice from different dietary groups (n=6 per group). C: Relative triglyceride (TG) content in different mouse groups (n=6 per group). D: Results of blood glucose and area under the curve (AUC) analysis using oral glucose tolerance test (OGTT) obtained for two strains of mice (n=6 per group). E: Blood glucose decay rate and AUC analysis of insulin tolerance test (ITT) results for two strains of mice (n=6 per group). F: Liver tissue pathological analysis using H&E staining (200× magnification) at different feeding time points. Scale bar: 25 μm. MAFLD activity scores were evaluated for each mouse (<3, no NASH; 3-5, borderline status; and >5, NASH). Red arrows indicate hepatocytes with ballooning degeneration. Yellow arrows indicate hepatic steatosis. Blue arrows indicate inflammatory cell infiltration. Data are means±*SEM*. *: P<0.05; **: P<0.01; ***: P<0.001; ****: P<0.0001. HFD: High-fat diet; HFFCD: High-fat, high-fructose, high-cholesterol diet; SD: Standard diet.

mice fed HFD or HFFCD diets from 8 weeks onward (Figure 1F). Based on the sum of scores for steatosis grade (0–3), lobular inflammation (0–3), and hepatocellular ballooning (0–2), which indicate NASH progression, we calculated the MAFLD activity score according to the NASH Clinical Research Network method (Kleiner et al, 2005). Results showed that the HFD- and HFFCD-fed mice exhibited severe hepatic injury characteristics with increased feeding time compared to the SD-fed mice, with the former reaching the NASH cutoff score of 5 by 18 weeks. Moreover, based on the MAFLD scores, the degree of steatosis was most severe in the HFFCD-fed mice compared to the two HFD-fed groups. These findings indicate that the consumption of HFD or HFFCD diets by B6 and D2 mice for 18 weeks led to progressive morphological and histological changes, similar to those observed in human NASH (Sanches et al., 2015).

Oxidative stress minimally changed during NASH progression

To assess oxidative stress changes occurring during NASH progression in our diet-induced models, we measured the relative levels of 8-OHdG, an indicator of oxidative DNA damage (Ichiba et al., 2003). As shown in Figure 2A, the levels of 8-OHdG were significantly higher in the B6 mice fed a HFD/HFFCD diet than the SD control mice from 12 weeks onward, suggesting DNA damage in the former. In D2 mice fed a HFD diet, the levels of 8-OHdG were significantly higher than those in SD mice at 8 and 12 weeks; however, no significant difference was observed at 18 weeks. Furthermore, dinitrophenol (DNP) levels, reflecting the intensity of protein carbonylation, did not differ significantly between the HFD- or HFFCD- and SD-fed mice, even at 18 weeks (Figure 2B, Supplementary Figure S2A). To evaluate whether the antioxidant mechanism played a key role in modulating protein oxidative stress, we next examined the expression of five antioxidant enzymes, i.e., cytosolic superoxide dismutase (SOD1), mitochondrial superoxide dismutase (SOD2), cytosolic catalase (CAT), peroxiredoxin with H_2O_2-scavenging function (PRDX1), and cytosolic thioredoxin (TRX), by western blot analyses in the mice fed different diets (Supplementary Figure S2B–D). Overall, no remarkable results were observed for the antioxidant enzymes, nor any significant differences found between the HFD/HFFCD- and paired SD-fed mice during the feeding period, suggesting that oxidative stress did not affect NASH progression in the mouse models.

Hepatic mitochondrial coupling efficiency decreased in mouse models with NASH features

To investigate whether mitochondrial function alterations were detectable in the livers of our mouse models, we measured the mitochondrial respiration capacity in liver tissues by *ex vivo* high-resolution respirometry (HRR). As shown in Figure 3A, the maximal respiration capacity was lower in the D2 HFD-fed mice than in the SD-fed mice from 8 weeks onward. Similar differences were observed in the levels of respiration supported by the combined complex I (glutamate

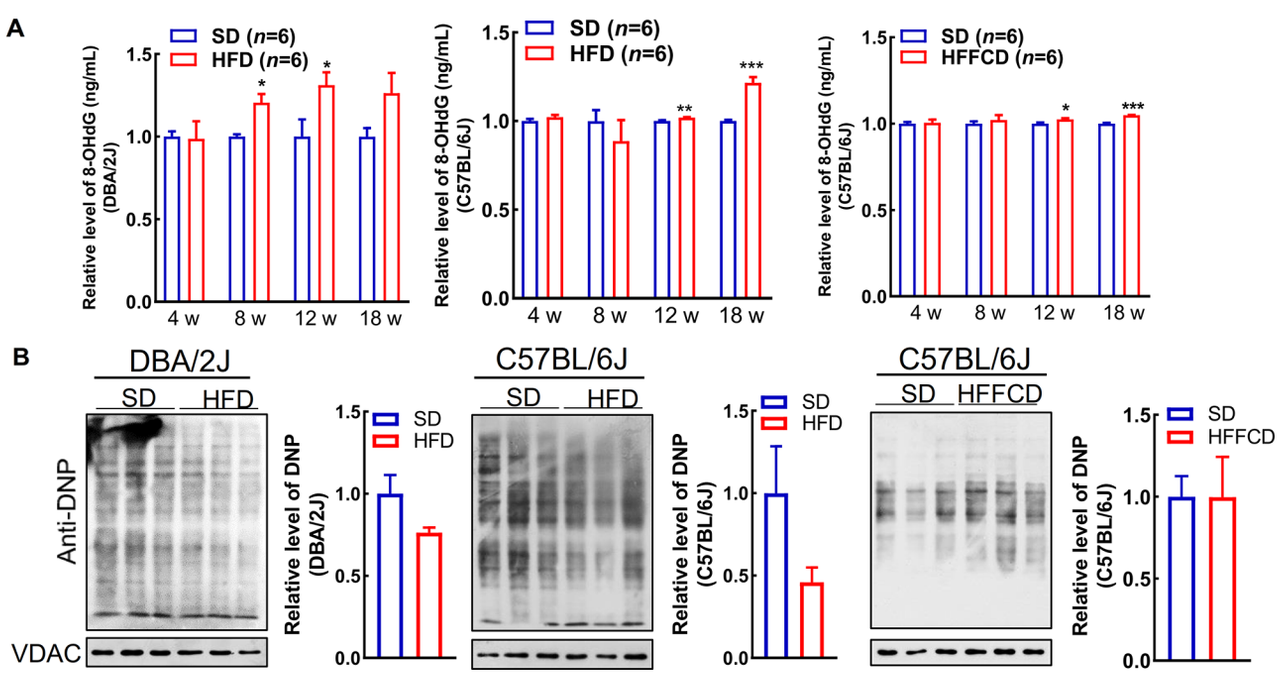

Figure 2 Oxidative stress and antioxidant markers during NASH progression

A: 8-Hydroxy-2′-deoxyguanosine (8-OHdG) levels in mouse liver tissue homogenates (n=6 per group). B: Protein carbonylation was measured using anti-DNP in liver tissues of mice (n=3 per group) fed HFD and HFFCD for 18 weeks. VDAC was used as internal control. Data are means±*SEM*. *: P<0.05; **: P<0.01; ***: P<0.001. HFD: High-fat diet; HFFC: High-fat, high-fructose, high-cholesterol diet; SD: Standard diet.

and malate) and II (succinate) substrates. Furthermore, the respiration supported by the combined complex I and II substrates were lower in the B6 HFD-fed mice compared to the SD-fed mice only at 4 weeks. In the B6 HFFCD-fed mice, the maximal respiratory capacity decreased at 4 and 12 weeks compared with that in the SD-fed mice, whereas the respiration supported by the combined complex I and II substrates showed a similar decrease at 12 weeks. Although not statistically significant in all groups, a slight decline in maximal respiratory capacity and combined complex I and II supported respiration were observed in the HFD- and HFFCD-fed mice. To examine whether the coupling of substrate oxidation to ATP production was impaired, we next assessed mitochondrial coupling efficiency using the respiratory control ratio (RCR) and leak control ratio (LCR). Results showed that RCR declined in the D2 HFD-fed mice compared with that in the SD-fed controls from 12 weeks onward, and LCR was higher in the D2 HFD-fed mice compared to the SD-fed mice at 8 and 12 weeks, suggesting mitochondrial uncoupling in HFD-fed mice. Similar RCR decreases were found in the B6 HFFCD-fed mice compared with SD-fed mice at 8 and 18 weeks (Figure 3B). No differences were observed in the LCR in B6 mice. However, not all gradual changes occurred across the time points, with decreases (13% in D2/HFD mice, 34% in B6/HFD mice, and 25% in B6/HFFCD mice) in RCR seen at 18 weeks in all HFD/HFFCD-fed mice compared with the corresponding SD-fed mice, suggesting that hepatic mitochondrial OXPHOS declined in the mouse models with NASH features. Subsequently, we measured the content and activities of the mitochondrial respiratory chain complexes using blue native PAGE and in-gel activity assay, respectively. However, no differences were observed in the content (Figure 3D, Supplementary Figure S3A–C) or activity (Figure 3E, Supplementary Figure S3D–F) of mitochondrial respiratory chain complexes between the HFD/HFFCD-fed mice and SD-fed controls, even at 18 weeks.

Hepatic transcriptome analysis of mouse models

To characterize transcriptional changes associated with mitochondrial function in NASH, transcript expression levels were analyzed in the livers of all mice using RNA sequencing. PCA of normalized data showed distinct clustering of the HFD/HFFCD-fed groups and SD-fed control group at all time

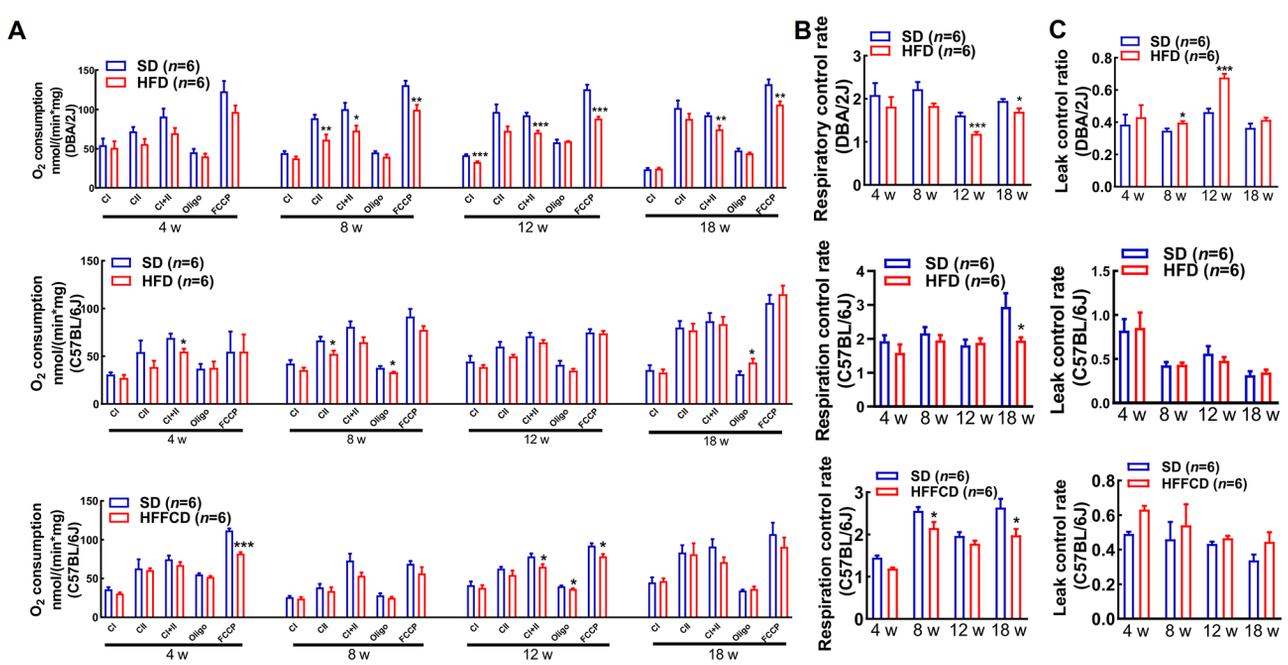

Figure 3 Hepatic mitochondrial function during NASH progression

A: Rates of oxygen fluxes in HFD-, HFFCD-, and SD-fed mice (n=6 per group) after 4, 8, 12, and 18 weeks of feeding. CI: respiration related to combined complex I activity, measured by presence of glutamate and malate; CII: respiration related to complex II activity, measured by presence of succinate; CI + II (state 3): respiration related to combined complex I and II activity, measured by presence of glutamate, malate, and succinate; Oligo (state o): uncoupled mitochondrial respiration, measured after adding oligomycin; FCCP (state u): maximum oxygen consumption, measured after adding FCCP. B: Evaluation of mitochondrial coupling using respiratory control ratio (RCR), defined as state 3/state o ratio. C: Evaluation of proton leakage using leak control ratio (LCR), defined as state o/state u ratio. D: Respiratory chain supercomplexes in HFD-, HFFCD-, and SD-fed mice (n=3 per group). Complexes I–V were probed in blue native PAGE-separated liver tissue lysates with antibodies against Grim19, SDHA, UQCRC2, COXI, and ATP5A, respectively. SC: Supercomplex. E: In-gel enzymatic activities of mitochondrial respiratory chain complexes I, II, IV, and V in HFD-, HFFCD-, and SD-fed mice (n=3 per group). SC: Supercomplex. Data are means±*SEM*. *: P<0.05; **: P<0.01; ***: P<0.001. HFD: High-fat diet; HFFCD: High-fat, high-fructose, high-cholesterol diet; SD: Standard diet.

points for B6 mice (Figure 4A). The D2/HFD- and SD-fed mice were not separated into distinct clusters at 4 and 8 weeks but were well separated from 12 weeks onward. With the SD-fed mice used as controls and an adjusted *P*-value of 5% applied to the data, the number of DEGs gradually decreased in the D2 mice from 1 094 at 4 weeks to 384 at 18 weeks (Figure 4B). Conversely, the B6 mice had the highest numbers of DEGs at 18 weeks, with the greatest number (2 271 DEGs) observed in the HFFCD-fed mice. Up-regulated and down-regulated DEGs were applied for GO and KEGG pathway analyses. Two pathways associated with inflammatory response, acute inflammatory response, and regulation of inflammatory response were up-regulated in the D2 HFD-fed mice compared with the SD group at 18 weeks (Figure 4C). Similar up-regulation was found in the B6 HFD-fed mice, with an additional up-regulated pathway (production of molecular mediator involved in inflammatory response). A more obvious up-regulation of inflammatory response-related pathways was observed in the HFFCD-fed mice, with five up-regulated pathways at 8 weeks and 10 up-regulated pathways by 18 weeks. These results demonstrate that inflammatory responses occurred in the HFD/HFFCD-fed mice, consistent with the data shown in Figure 1F.

We also analyzed the pathways related to oxidative stress and mitochondrial function; however, no changes were observed in these pathways in the D2 mice. Meanwhile, the response to the oxidative stress pathway was down-regulated at 4 weeks in the B6 HFD-fed mice, and a similar decrease was observed at 8 weeks in the HFFCD-fed mice. An additional pathway (regulation of the response to oxidative stress) was up-regulated in the HFFCD-fed mice at 18 weeks, which may have been a response to a more severe phenotype caused by the high dietary fructose and cholesterol (Figure 4D). Analyses of the pathways associated with

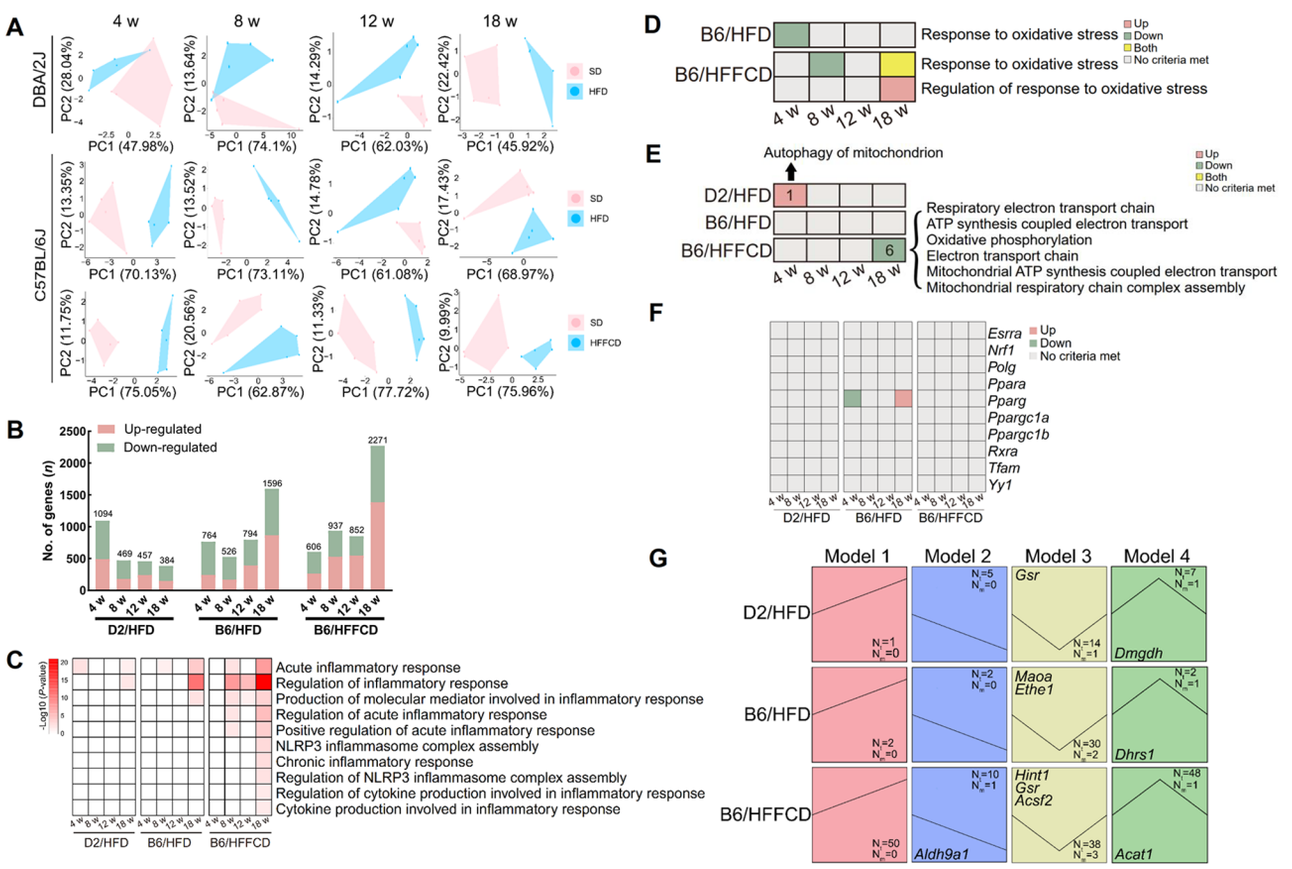

Figure 4 Hepatic transcriptome profiling during NASH progression

A: Principal component analysis of data obtained for different groups (n=5 per group) at different time points. B: Number of differentially expressed genes (DEGs) in different groups at different time points. C: Up-regulated pathways associated with inflammatory responses in different groups at different time points. D: Pathways associated with oxidative stress in different groups at different time points. E: Pathways associated with mitochondrial function in different groups at different time points. F: Heatmap showing DEGs encoding transcription factors affecting mitochondrial biogenesis. G: Simulation of four gene models using four possible gene expression trends (continuous rising; continuous falling; falling and then rising; and rising and then falling) to identify involved mitochondrial genes. HFD: High-fat diet; HFFCD: High-fat, high-fructose, high-cholesterol diet; SD: Standard diet.

mitochondrial function indicated that autophagy of the mitochondrial pathway was enhanced at 4 weeks in the D2 HFD-fed mice, suggesting mitochondrial impairment due to HFD (Figure 4E). Nevertheless, no other up-regulated pathway was found to be associated with impaired mitochondrial function in the two HFD-fed groups over the feeding period. However, a total of six pathways, including OXPHOS, were down-regulated at 18 weeks in the HFFCD-fed mice, providing evidence of a decline in mitochondrial function with NASH progression to a high histological grade (Figure 3A). It is possible that pathway analysis was affected by the number of DEGs, as we manually selected genes related to mitochondrial function. Most OXPHOS genes encoded by both nuclear DNA (Supplementary Figure S4A) and mitochondrial DNA (Supplementary Figure S4B) did not differ significantly in D2/HFD and B6/HFD mice compared with SD-fed mice. Notably, there were relatively large numbers of down-regulated genes in the B6/HFFCD group, consistent with the pathway analysis presented in Figure 4E. However, after generating a heatmap for genes associated with the mitochondrial quality control system, no significant changes were observed in genes related to mitochondrial damage, including those associated with fusion (*Mfn1*, *Mfn2*), fission (*Dnm1l*, *Oma1*, *Opa1*), and mitophagy (*Pink1*, *Prkn*). In addition, we profiled gene expression of transcription factors involved in mitochondrial biogenesis and found that the expression of most genes remained unchanged in the HFD/HFFCD-fed mice, demonstrating that mitochondrial biogenesis was minimally affected during NASH progression (Figure 4F).

To further explore changes in mitochondrial function during NASH progression, we simulated four possible gene expression trends, namely, continuous rising, continuous falling, falling and then rising, and rising and then falling, and identified the associated mitochondrial genes according to the MitoCarta 2.0 database (Figure 4G). For the D2 mice, *Gsr* was involved in model 3 and *Dmgdh* was associated with model 4. For the B6 HFD-fed mice, two genes, *Maoa* and *Ethe1*, were involved in model 3, and one gene, *Dhrs1*, was associated with model 4. For the B6 HFFCD-fed mice, *Aldh9a1* was found in model 2; *Hint1*, *Gsr*, and *Acsf2* were found in model 3; and *Acat1* was found in model 4. Pathway analyses showed that no pathway was associated with mitochondrial function in any model, further implying a weak association between NASH progression and mitochondrial dysfunction.

Hepatic transcriptome analysis of public human NASH dataset

To verify the above conclusions, we downloaded and re-analyzed a public liver transcriptome dataset for individuals with a healthy normal weight, individuals classified as obese (Obese), individuals with simple steatosis (NAFL), and individuals with NASH from the GEO database. A PCA plot indicated distinct clustering of the NC group from the NAFL and NASH groups, while neither the Obese and NC group, nor the NAFL and NASH group could be separated into clusters (Figure 5A). These findings indicate that there was an unclear boundary between NAFL and NASH. Similarly, DEG analysis identified 116 DEGs between NAFL and NASH, and 41 DEGs between Obese and NC, accounting for far fewer than the 5 759 DEGs between NAFL and NC and 6 697 DEGs between NASH and NC (Figure 5B). Subsequently, GO and KEGG pathway analyses were performed for DEGs in each comparison group. Although we found several significant regulated pathways (Figure 5C, Supplementary Table S1) in NAFL or NASH compared with NC, such as the RAP1 signaling pathway, no pathways related to mitochondrial function were identified in any comparison group. These data provide further support for the weak association between MAFLD progression and mitochondrial dysfunction.

DISCUSSION

Diet-induced mouse models have been widely used to investigate the progression of MAFLD and NASH (Friedman et al, 2018) as they allow for simulation of the occurrence and progression of MAFLD/NASH within a relatively short time, unlike that in human subjects. These models also circumvent the strict ethical limitations that exist in collecting liver tissue samples from human patients (Takahashi et al, 2012). The C57BL/6 mouse strain is generally preferred due to its intrinsic predisposition to developing obesity and MAFLD (Kohli & Feldstein, 2011). However, due to a limited feeding time duration, systematic analysis of pathological changes occurring during NASH progression has proven challenging in previous studies. Hence, in the current study we employed a comprehensive multi-time-point design with two mouse strains maintained on different diets. Two obese NASH progression models were constructed by feeding B6 mice with a HFD or HFFCD diet for 4, 8, 12, and 18 weeks. Histopathological examination of H&E-stained liver tissue confirmed that the pathology (steatosis, ballooning degeneration, and hepatic inflammation) of the B6 HFD/HFFCD-fed mice was similar to that in human NASH (Sanches et al., 2015). Moreover, we established a NASH progression model in D2 mice using the same feeding method as that for B6 HFD-fed mice. Higher insulin sensitivity was observed in the D2 HFD-fed mice compared to the SD-fed mice from 8 weeks onward; however, the B6 mice did not show the same phenomenon until 18 weeks, indicating higher sensitivity to obesogenic diets in D2 mice (Hansen et al, 2017; Zhu et al, 2009) and advantages in diet-induced model construction related to liver disease, as reported previously (Kanuri & Bergheim, 2013). Among the three different models used, the HFFCD-fed mice experienced more severe steatosis and had a higher MAFLD activity score than the HFD-fed mice. Furthermore, transcriptome analysis suggested that there were far more up-regulated pathways associated with inflammatory responses in the HFFCD-fed mice, consistent with previous data showing that high consumption of fructose and cholesterol can increase MAFLD severity by worsening fat accumulation, insulin resistance, and inflammation (Liang et al, 2018).

Many recent studies have shown that oxidative stress is an important factor in the progression of steatosis to steatohepatitis (Borrelli et al, 2018). Elevated hepatic levels of 8-OHdG, a marker of mitochondrial oxidized DNA, have been observed in patients with MAFLD and NASH (Seki et al, 2002; Tanaka et al, 2013), suggesting increased oxidative DNA damage targeting mitochondrial function. In the present study, we found similarly increased levels of 8-OHdG in the HFD/HFFCD-fed mice compared to the SD-fed mice. However, unlike the redox imbalance found in patients with NASH (Paradies et al, 2014; Rolo et al, 2012; Song et al, 2013), we found that the oxidative and antioxidant capacities were not affected in the HFD/HFFCD-fed mice compared to the SD-fed mice. These findings may have resulted from our using liver mitochondria to measure protein carbonylation and antioxidant enzymes so that the data represented oxidative and antioxidant capacities in isolated mitochondria rather than in hepatocytes. Moreover, transcriptome expression profiling showed that the expressions of several genes involved in antioxidant activity, such as *Gpx4*, *Sod1*, and *Txnrd1*, were significantly lower in the HFD- and HFFCD-fed mice than in the SD-fed mice; however, the fold-changes in gene expression were rather small (less than 1.5; Supplementary Figure S4D). Therefore, it is likely that the differences in gene

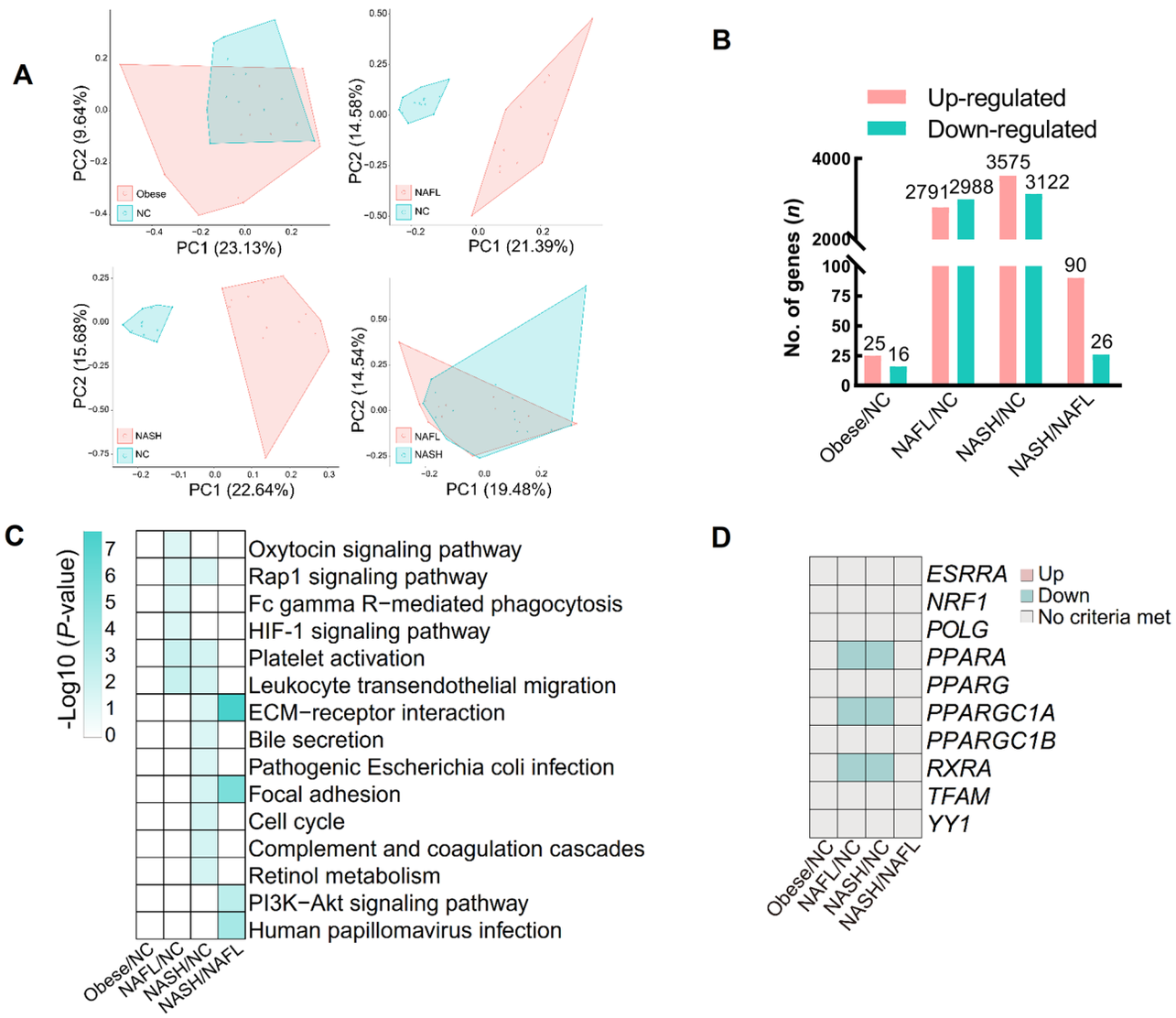

Figure 5 Hepatic transcriptome analysis of public human NASH dataset

A: Principal component analysis of extracted data for four comparison groups (Obese relative to NC (Obese/NC), NAFL relative to NC (NAFL/NC), NASH relative to NC (NASH/NC), NASH relative to NAFL (NASH/NAFL)). B: Number of differentially expressed genes (DEGs) in each comparison group. C: KEGG pathway analysis of DEGs in each comparison group. D: Heatmap showing DEGs encoding transcription factors affecting mitochondrial biogenesis.

expression were not reflected in protein expression. Overall, oxidative damage to mitochondrial proteins remained unchanged in the livers of mice during MAFLD development, indicating that hepatic mitochondrial oxidative stress was not associated with progression of obesity-induced MAFLD.

Several recent studies have suggested that mitochondrial dysfunction plays a key role in the development of MAFLD. For instance, (Koliaki et al, 2015) reported that increased mitochondrial respiration in individuals with NAFL is not found in body mass index (BMI)-matched individuals with NASH. The authors suggest that increased hepatic lipid utilization in patients with NAFL could stimulate the capacity of liver mitochondria, thereby preventing MAFLD progression. Other studies have reported decreased mitochondrial oxidative capacity in the liver tissue of patients and animal models with hepatic steatosis (Garcia-Ruiz et al, 2006; Perez-Carreras et al, 2003), yet have not consistently observed this effect in NASH patients (Begriche et al, 2006). In the current study, we found a similarly significant yet mild decrease in hepatic mitochondrial respiration in some HFD/HFFCD-fed mice compared to SD-fed mice. Methodological issues, or a lack of proper correction for mitochondrial content, are likely the primary causes for the observed differences in results. Alternatively, direct measurement of a great number of fresh tissues is the primary limitation for human samples during HRR (Schopf et al, 2016). In addition, it is not appropriate to use citrate synthase activity (CSA) for the correction of mitochondrial content in MAFLD studies due to the unclear association between CSA and mitochondrial content (Lund et al, 2016). Hence, although we observed the citrate cycle to be down-regulated at certain time points in our models (Supplementary Figure S4E), we used mitochondrial protein concentration for correction to obtain the respiration capacity per mitochondrion. Moreover, rather than detecting oxidation metabolism through *in vivo* $^{2}H/^{13}C$ tracer methods (Satapati et al, 2015; Satapati et al, 2012), we used HRR to obtain the maximal mitochondrial OXPHOS capacity with excess substrates and ADP in isolated hepatic mitochondria. This approach, in some regards, ignores factors affecting mitochondrial function *in vivo*, such as substrate abundance, hormonal levels, and intracellular and intercellular mitochondrial dynamics, leading to variable results (Stirone et al, 2005; Valdinocci et al, 2019; Zhdanov et al, 2014).

High-throughput sequencing technologies have been widely used to explore the associated metabolic pathways and functional genes involved in the development of MAFLD. (Krishnan et al, 2018) and (Peng et al, 2018) performed transcriptomic and lipidomic analysis of liver samples from humans and mice with MAFLD and identified mitochondrial dysfunction as the driving force for the progression of MAFLD. In this study, we performed transcriptome sequencing of liver samples in each comparison group and analyzed the pathways and genes associated with mitochondrial function, and only found a weak association between mitochondrial function and the development of MAFLD. The limitations of Krishnan et al. (2018) and our study were the use of liver samples mixed with hepatocytes and hepatic nonparenchymal cells for transcriptome sequencing, and indeed differences in manual tissue sampling may account for some of the discrepancies between these reports. In Krishnan et al. (2018), data collection and key driver (KD) genes were obtained from multiple mouse strains fed a HF/HS diet for 8 weeks, and knockdown of KD genes in AML12 cells showed decreased mitochondrial respiration. Thus, the authors highlighted mitochondrial dysfunction as a key mechanistic driver of MAFLD. As there was no detection of mitochondrial function in samples from mice with knockdown of KD genes by Krishnan et al. (2018), we are not sure about the effect of KD genes on mitochondrial function *in vivo* or *ex vivo*. Moreover, we selected these KD genes in our transcriptome data (Supplementary Table S2) but did not find similar or consistent changes of these genes in our models. As MAFLD is comprised of both obese and non-obese MAFLD, these genes might be regulated differently in the different subtypes. As we used obese models only, at least for diet-induced obese MAFLD, we concluded that mitochondrial dysfunction does not appear to be the driving force of the disease.

Mitochondria have been proposed as a promising therapeutic target for metabolic disorders due to their pivotal role in the regulation of energy homeostasis. Despite the assessment of several mitochondrial agents in humans, such as CoQ10 for heart failure and MitoQ for chronic kidney disease (Murphy & Hartley, 2018), treatment options for MAFLD remain limited. Our results indicate that mitochondrial dysfunction is not closely associated with progression of MAFLD, at least in diet-induced obese mouse models. Therefore, considering that MAFLD does not discriminate between obese and non-obese individuals, it seems prudent to reassess treatment strategies to consider those that would prove effective in all MAFLD patient subtypes.

In conclusion, our study demonstrated a slight decline in mitochondrial function in the histological evolution of NASH. Although this study was cross-sectional, the multiplicity of observations provides some insight into disease progression. Based on the comprehensive analysis of the mitochondrial function in multiple obesity-induced MAFLD models, as well as in human individuals with or without NASH, our results imply that impaired hepatic mitochondrial function is not closely associated with the development of MAFLD. Thus, therapeutic strategies targeting mitochondria for the treatment of MAFLD should be reconsidered.

SUPPLEMENTARY DATA

Supplementary data to this article can be found online.

COMPETING INTERESTS

The authors declare that they have no competing interests.

AUTHORS' CONTRIBUTIONS

H.Z.F., and J.X.L. planned the project and designed the

experiments. L.H.G. performed the mouse studies. L.H.G., K.Z., H.F.C., X.X.Z., Q.L.D., Y.Z., and H.B.Z. performed the biochemical experiments. Q.Y.Z. performed the transcriptome studies. H.Z.F. and Q.Y.Z. wrote the manuscript. All authors read and approved the final version of the manuscript.

ACKNOWLEDGMENTS

We thank Ping Yang and Jun Ma (First Affiliated Hospital of Wenzhou Medical University) for assistance in the assessment of MAFLD activity scores.

REFERENCES

Bechmann LP, Gastaldelli A, Vetter D, Patman GL, Pascoe L, Hannivoort RA, et al. 2012a. Glucokinase links Krüppel-like factor 6 to the regulation of hepatic insulin sensitivity in nonalcoholic fatty liver disease. *Hepatology*, **55**(4): 1083−1093.

Bechmann LP, Hannivoort RA, Gerken G, Hotamisligil GS, Trauner M, Canbay A. 2012b. The interaction of hepatic lipid and glucose metabolism in liver diseases. *Journal of Hepatology*, **56**(4): 952−964.

Begriche K, Igoudjil A, Pessayre D, Fromenty B. 2006. Mitochondrial dysfunction in NASH: causes, consequences and possible means to prevent it. *Mitochondrion*, **6**(1): 1−28.

Borrelli A, Bonelli P, Tuccillo FM, Goldfine ID, Evans JL, Buonaguro FM, et al. 2018. Role of gut microbiota and oxidative stress in the progression of non-alcoholic fatty liver disease to hepatocarcinoma: current and innovative therapeutic approaches. *Redox Biology*, **15**: 467−479.

Eslam M, Sanyal AJ, George J, International Consensus Panel. 2020. MAFLD: a consensus-driven proposed nomenclature for metabolic associated fatty liver disease. *Gastroenterology*, **158**(7): 1999−2014.

Fabbrini E, Mohammed BS, Magkos F, Korenblat KM, Patterson BW, Klein S. 2008. Alterations in adipose tissue and hepatic lipid kinetics in obese men and women with nonalcoholic fatty liver disease. *Gastroenterology*, **134**(2): 424−431.

Fang HZ, Hu NQ, Zhao QY, Wang BQ, Zhou HB, Fu QZ, et al. 2018. mtDNA Haplogroup N9a increases the risk of type 2 diabetes by altering mitochondrial function and intracellular mitochondrial signals. *Diabetes*, **67**(7): 1441−1453.

Franko A, Von Kleist-Retzow JC, Neschen S, Wu MY, Schommers P, Bose M, et al. 2014. Liver adapts mitochondrial function to insulin resistant and diabetic states in mice. *Journal of Hepatology*, **60**(4): 816−823.

Friedman SL, Neuschwander-Tetri BA, Rinella M, Sanyal AJ. 2018. Mechanisms of NAFLD development and therapeutic strategies. *Nature Medicine*, **24**(7): 908−922.

Garcia-Ruiz C, Baulies A, Mari M, Garcia-Rovés PM, Fernandez-Checa JC. 2013. Mitochondrial dysfunction in non-alcoholic fatty liver disease and insulin resistance: cause or consequence?. *Free Radical Research*, **47**(11): 854−868.

Garcia-Ruiz I, Rodríguez-Juan C, Díaz-Sanjuan T, Del Hoyo P, Colina F, Muñoz-Yagüe T, et al. 2006. Uric acid and anti-TNF antibody improve mitochondrial dysfunction in ob/ob mice. *Hepatology*, **44**(3): 581−591.

Hansen HH, Feigh M, Veidal SS, Rigbolt KT, Vrang N, Fosgerau K. 2017. Mouse models of nonalcoholic steatohepatitis in preclinical drug development. *Drug Discovery Today*, **22**(11): 1707−1718.

Hijona E, Hijona L, Arenas JI, Bujanda L. 2010. Inflammatory mediators of hepatic steatosis. *Mediators of Inflammation*, **2010**: 837419.

Ichiba M, Maeta Y, Mukoyama T, Saeki T, Yasui S, Kanbe T, et al. 2003. Expression of 8-hydroxy-2'-deoxyguanosine in chronic liver disease and hepatocellular carcinoma. *Liver International*, **23**(5): 338−345.

Kanuri G, Bergheim I. 2013. *In vitro* and *in vivo* models of non-alcoholic fatty liver disease (NAFLD). *International Journal of Molecular Sciences*, **14**(6): 11963−11980.

Kleiner DE, Brunt EM, Van Natta M, Behling C, Contos MJ, Cummings OW, et al. 2005. Design and validation of a histological scoring system for nonalcoholic fatty liver disease. *Hepatology*, **41**(6): 1313−1321.

Kohli R, Feldstein AE. 2011. NASH animal models: *are we there yet*?. *Journal of Hepatology*, **55**(4): 941−943.

Koliaki C, Szendroedi J, Kaul K, Jelenik T, Nowotny P, Jankowiak F, et al. 2015. Adaptation of hepatic mitochondrial function in humans with non-alcoholic fatty liver is lost in steatohepatitis. *Cell Metabolism*, **21**(5): 739−746.

Kopec KL, Burns D. 2011. Nonalcoholic fatty liver disease: a review of the spectrum of disease, diagnosis, and therapy. *Nutrition in Clinical Practice*, **26**(5): 565−576.

Krishnan KC, Kurt Z, Barrere-Cain R, Sabir S, Das A, Floyd R, et al. 2018. Integration of multi-omics data from mouse diversity panel highlights mitochondrial dysfunction in non-alcoholic fatty liver disease. *Cell Systems*, **6**(1): 103−115.

Liang JQ, Teoh N, Xu LX, Pok S, Li XC, Chu ESH, et al. 2018. Dietary cholesterol promotes steatohepatitis related hepatocellular carcinoma through dysregulated metabolism and calcium signaling. *Nature Communications*, **9**(1): 4490.

Lund MT, Kristensen M, Hansen M, Tveskov L, Floyd AK, Støckel M, et al. 2016. Hepatic mitochondrial oxidative phosphorylation is normal in obese patients with and without type 2 diabetes. *The Journal of Physiology*, **594**(15): 4351−4358.

Lund MT, Larsen S, Hansen M, Courraud J, Floyd AK, Stockel M, et al. 2018. Mitochondrial respiratory capacity remains stable despite a comprehensive and sustained increase in insulin sensitivity in obese patients undergoing gastric bypass surgery. *Acta Physiologica*, **223**(1): e13032.

Murphy MP, Hartley RC. 2018. Mitochondria as a therapeutic target for common pathologies. *Nature Reviews Drug Discovery*, **17**(12): 865−886.

Neuschwander-Tetri BA. 2010. Hepatic lipotoxicity and the pathogenesis of nonalcoholic steatohepatitis: the central role of nontriglyceride fatty acid metabolites. *Hepatology*, **52**(2): 774−788.

Paradies G, Paradies V, Ruggiero FM, Petrosillo G. 2014. Oxidative stress, cardiolipin and mitochondrial dysfunction in nonalcoholic fatty liver disease. *World Journal of Gastroenterology*, **20**(39): 14205−14218.

Peng KY, Watt MJ, Rensen S, Greve JW, Huynh K, Jayawardana KS, et al. 2018. Mitochondrial dysfunction-related lipid changes occur in nonalcoholic fatty liver disease progression. *Journal of Lipid Research*, **59**(10): 1977−1986.

Pérez-Carreras M, Del Hoyo P, Martin MA, Rubio JC, Martin A, Castellano G, et al. 2003. Defective hepatic mitochondrial respiratory chain in patients with nonalcoholic steatohepatitis. *Hepatology*, **38**(4): 999−1007.

Rector RS, Thyfault JP, Uptergrove GM, Morris EM, Naples SP, Borengasser SJ, et al. 2010. Mitochondrial dysfunction precedes insulin

resistance and hepatic steatosis and contributes to the natural history of non-alcoholic fatty liver disease in an obese rodent model. *Journal of Hepatology*, **52**(5): 727−736.

Rolo AP, Teodoro JS, Palmeira CM. 2012. Role of oxidative stress in the pathogenesis of nonalcoholic steatohepatitis. *Free Radical Biology and Medicine*, **52**(1): 59−69.

Sanches SC, Ramalho LN, Augusto MJ, Da Silva DM, Ramalho FS. 2015. Nonalcoholic steatohepatitis: a search for factual animal models. *BioMed Research International*, **2015**: 574832.

Satapati S, Kucejova B, Duarte JAG, Fletcher JA, Reynolds L, Sunny NE, et al. 2015. Mitochondrial metabolism mediates oxidative stress and inflammation in fatty liver. *The Journal of Clinical Investigation*, **125**(12): 4447−4462.

Satapati S, Sunny NE, Kucejova B, Fu XR, He TT, Méndez-Lucas A, et al. 2012. Elevated TCA cycle function in the pathology of diet-induced hepatic insulin resistance and fatty liver. *Journal of Lipid Research*, **53**(6): 1080−1092.

Schöpf B, Schäfer G, Weber A, Talasz H, Eder IE, Klocker H, et al. 2016. Oxidative phosphorylation and mitochondrial function differ between human prostate tissue and cultured cells. *The FEBS Journal*, **283**(11): 2181−2196.

Seki S, Kitada T, Yamada T, Sakaguchi H, Nakatani K, Wakasa K. 2002. In situ detection of lipid peroxidation and oxidative DNA damage in non-alcoholic fatty liver diseases. *Journal of Hepatology*, **37**(1): 56−62.

Silva AM, Oliveira PJ. 2012. Evaluation of respiration with clark type electrode in isolated mitochondria and permeabilized animal cells. *In*: Palmeira CM, Moreno AJ. Mitochondrial Bioenergetics. New York: Humana Press, 7–24.

Simões ICM, Fontes A, Pinton P, Zischka H, Wieckowski MR. 2018. Mitochondria in non-alcoholic fatty liver disease. *The International Journal of Biochemistry & Cell Biology*, **95**: 93−99.

Song BJ, Abdelmegeed MA, Henderson LE, Yoo SH, Wan J, Purohit V, et al. 2013. Increased nitroxidative stress promotes mitochondrial dysfunction in alcoholic and nonalcoholic fatty liver disease. *Oxidative Medicine and Cellular Longevity*, **2013**: 781050.

Stirone C, Duckles SP, Krause DN, Procaccio V. 2005. Estrogen increases mitochondrial efficiency and reduces oxidative stress in cerebral blood vessels. *Molecular Pharmacology*, **68**(4): 959−965.

Sun DY, Li B, Qiu RY, Fang HZ, Lyu J. 2016. Cell type-specific modulation of respiratory Chain Supercomplex organization. *International Journal of Molecular Sciences*, **17**(6): 926.

Takahashi Y, Soejima Y, Fukusato T. 2012. Animal models of nonalcoholic fatty liver disease/nonalcoholic steatohepatitis. *World Journal of Gastroenterology*, **18**(19): 2300−2308.

Tanaka S, Miyanishi K, Kobune M, Kawano Y, Hoki T, Kubo T, et al. 2013. Increased hepatic oxidative DNA damage in patients with nonalcoholic steatohepatitis who develop hepatocellular carcinoma. *Journal of Gastroenterology*, **48**(11): 1249−1258.

Tilg H, Moschen A. 2010. Update on nonalcoholic fatty liver disease: genes involved in nonalcoholic fatty liver disease and associated inflammation. *Current Opinion in Clinical Nutrition and Metabolic Care*, **13**(4): 391−396.

Valdinocci D, Simões RF, Kovarova J, Cunha-Oliveira T, Neuzil J, Pountney DL. 2019. Intracellular and intercellular mitochondrial dynamics in Parkinson's disease. *Frontiers in Neuroscience*, **13**: 930.

Younossi Z, Anstee QM, Marietti M, Hardy T, Henry L, Eslam M, et al. 2018. Global burden of NAFLD and NASH: trends, predictions, risk factors and prevention. *Nature Reviews Gastroenterology & Hepatology*, **15**(1): 11−20.

Zhdanov AV, Waters AHC, Golubeva AV, Dmitriev RI, Papkovsky DB. 2014. Availability of the key metabolic substrates dictates the respiratory response of cancer cells to the mitochondrial uncoupling. *Biochimica et Biophysica Acta (BBA) - Bioenergetics*, **1837**(1): 51−62.

Zhou F, Zhou JH, Wang WX, Zhang XJ, Ji YX, Zhang P, et al. 2019. Unexpected rapid increase in the burden of NAFLD in China From 2008 to 2018: a systematic review and meta-analysis. *Hepatology*, **70**(4): 1119−1133.

Zhu MZ, Ji GZ, Jin G, Yuan ZB. 2009. Different responsiveness to a high-fat/cholesterol diet in two inbred mice and underlying genetic factors: a whole genome microarray analysis. *Nutrition & Metabolism*, **6**(1): 43.